Published in final edited form as:
Nature. 2018 December 01; 564(7734): 77–82. doi:10.1038/s41586-018-0693-y.

Type 9 secretion system structures reveal a new protein transport mechanism

Frédéric Lauber[#1], **Justin C. Deme**[#2,3], **Susan M. Lea**[2,3,†], **Ben C. Berks**[1,†]

[1]Department of Biochemistry, University of Oxford, South Parks Road, Oxford OX1 3QU, United Kingdom

[2]Sir William Dunn School of Pathology, University of Oxford, South Parks Road, Oxford OX1 3RE, United Kingdom

[3]The Central Oxford Structural Molecular Imaging Centre (COSMIC), University of Oxford, South Parks Road, Oxford OX1 3RQ, United Kingdom

[#] These authors contributed equally to this work.

Summary

The Type IX Secretion system (T9SS) is the protein export pathway of bacteria of the Gram-negative *Fibrobacteres-Chlorobi-Bacteroidetes* superphylum and is an essential pathogenicity determinant in severe periodontal disease. The central element of the T9SS is a so far uncharacterized protein-conducting translocon located in the bacterial outer membrane. Using cryo-electron microscopy we now provide structural evidence that the translocon is the T9SS protein SprA. SprA forms an unprecedentedly large (36-strand) single polypeptide transmembrane β-barrel. The barrel pore is capped on the extracellular end, but has a lateral opening to the external membrane surface. Structures of SprA bound to different T9SS components demonstrate that partner proteins control access to the lateral opening and to the periplasmic end of the pore. Our results uncover a protein transporter of distinctive architecture that operates a novel alternating access mechanism in which the two ends of the protein conducting channel are open at different times.

The Type IX Secretion System (T9SS) is responsible for protein export across the outer membrane of bacteria of the *Fibrobacteres-Chlorobi-Bacteroidetes* (FCB) superphylum[1,2].

[†]Correspondence and requests for material should be addressed to S.M.Lea (susan.lea@path.ox.ac.uk); B.C.Berks (ben.berks@bioch.ox.ac.uk).

Data availability

The cryo-EM density maps have been deposited in the World Wide Protein Data Bank (wwPDB) under accession codes EMD-0133 and EMD-0134, and the coordinates have been deposited in the Protein Data Bank (PDB) under accession numbers 6h3i and 6h3j. Source Data for Figs. 1d and 4a, b are available with the online version of the paper.

Author contributions

F.L. carried out all genetic and biochemical work. J.C.D. collected EM data. J.C.D. and S.M.L. determined the structure. B.C.B. conceived the project. All authors interpreted data and wrote the manuscript.

Author Information

Reprints and permissions information is available at www.nature.com/reprints.

The authors declare no competing interests.

Readers are welcome to comment on the online version of the paper.

Europe PMC Funders Author Manuscripts

In *Porphyromonas gingivalis* and related human oral pathogens that are the cause of severe periodontal disease, the T9SS is an essential virulence determinant [2]. The T9SS is also a pathogenicity factor in major bacterial diseases of farmed fish, including columnaris disease and cold-water disease[3,4]. Bacteroidetes exhibit a unique and rapid gliding motility in which cell surface adhesins move on helical tracks[5]. This gliding motility is intimately linked to the T9SS through the involvement of the T9SS in adhesin export and possibly through the use of a shared motor complex[6].

T9SS substrates are large (100-650kDa) multi-domain proteins which fold in the periplasm before being exported through an outer membrane translocon. Substrates are targeted to the translocon by means of a ca. 100 amino acid C-terminal folded signal domain (CTD)[7,8]. Distinct Type A and Type B CTDs have been defined and these exhibit some differences in the T9SS components required for their export[1,8,9].

The Bacteroidete T9SS contains at least 15 proteins[1,2,10]. The GldKLMN proteins form a trans-periplasmic motor complex that is thought to use the inner membrane protonmotive force to drive secretion at the outer membrane[11,12]. The PorQUVZ proteins form a cell surface-exposed Attachment Complex[13] which proteolytically removes the substrate CTD following transport[14] and covalently links some substrate proteins to a lipopolysaccharide anchor[15]. A pool of PorV proteins in the outer membrane is thought to shuttle substrate proteins from the translocon to the Attachment Complex[13]. The functions of the remaining T9SS components are unclear. In particular, the identities of the components which form the outer membrane translocon itself have been completely unknown.

We reasoned that the protein-conducting channel of the T9SS translocon must be formed by a protein that traverses the outer membrane. However, most of the outer membrane-spanning T9SS components can be predicted to form β-barrels of 14 or fewer strands, with internal pores that would be too narrow to accommodate the folded T9SS substrate proteins. The one exception is the protein SprA (also termed Sov), a 267kDa polypeptide with no sequence similarity to other currently identified proteins[16,17]. This logic led us to hypothesise that SprA forms the protein-conducting channel of the T9SS translocon. In support of this contention, we note that the protein forming the transport channel would also be expected to be one of the five Bacteroidete T9SS components (SprA, SprE, PorU, PorV, and PorZ) that are retained in a minimal T9SS found in other members of the FCB superphylum ([18] and our analysis).

Characterization of SprA

We constructed strains of the gliding bacterium *Flavobacterium johnsoniae* in which the SprA protein was fused to either a HaloTag domain, to allow fluorophore labelling, or to a Twin-Strep tag, to permit affinity purification. These strains retain full T9SS function (Extended Data Fig. 1a-d and Supplementary Video 1).

The fluorophore-labelled SprA fusion localizes to an average of 7 ± 2SD well-resolved foci per cell (314 cells, Fig. 1a, b). Photobleaching traces show that most foci contain a single SprA molecule (1.2 ± 0.4SD photobleaching steps per focus using 119 traces, Fig. 1c). The

SprA foci are stationary with respect to the cell body in both immobile and gliding cells (Supplementary Video 2). Thus, SprA is not physically linked to the mobile cell surface adhesins.

We used the Twin-Strep-tagged SprA fusion to isolate SprA from otherwise native cells. Proteomics analysis of the SprA preparation showed that the majority of the purified SprA molecules are proteolytically clipped between residues 1905 and 1946 (Fig. 1d and Extended Data Fig. 1e). We found that SprA co-purifies with the known T9SS component PorV as well as two additional proteins, Fjoh_1759 and Fjoh_4997 (Fig. 1d). Fjoh_4997 is a lipoprotein peptidyl-prolyl *cis-trans* isomerase of the FKBP superfamily, hereafter referred to as PPI. Fjoh_1759 is a protein of unknown function but with a phylogenetic distribution that strongly correlates with the presence of a T9SS [10]. For reasons set out below, we term Fjoh_1759 the Plug protein.

Cryo-electron microscopy was used to determine the structure of two, distinct, complexes in which SprA associates either with the PPI and PorV proteins (PorV complex) or the PPI and Plug proteins (Plug complex)(Fig. 1e-g, Extended Data Table 1, Extended Data Fig. 2, Supplementary Videos 3, 4). Fourier Shell Correlation (FSC) defines the resolution of the PorV complex as 3.5 Å overall (local resolution varying from 3.3-5.0 Å) whilst the Plug complex is at a resolution of 3.7 Å (local resolution 3.4-4.7 Å)(Extended Data Fig. 2c, d). For both complexes an α-carbon trace was initially built through the EM volume. Regions corresponding to PorV, PPI, and Plug were assigned by dissecting the EM volume into domains and searching the PDB for structural homologues (Extended Data Fig. 3a). Sequences could be docked into these regions of the structures guided by the identified homologues. Sequence docking was then extended manually into SprA (Extended Data Fig. 2e). With the exception of ~100 amino acids at the N-terminus of SprA and some short disordered loops, the chains were continuously traced.

SprA and PorV both form transmembrane β-barrels (Fig. 1g). This allowed us to assign the orientation of the SprA complexes in the outer membrane based on the principle that the last β-strand of bacterial single subunit β-barrel proteins is always at the periplasmic side of the membrane[19]. The site at which proteolytic clipping occurs during purification of SprA falls within a 50 residue loop that extends from the periplasmic side of the SprA barrel between strands 24 and 25. This loop is not visible in the EM density for either of our two complexes.

SprA architecture

Using the location of the detergent associated with the complexes to define the likely plane of the membrane, the SprA barrel extends ~20 Å above the membrane on the extracellular side of the complex (Fig. 1e). Two large, folded inserts between barrel strands 7/8 and 11/12 form a 50 Å high cap structure that seals the extracellular end of the barrel. Each of the two cap inserts is composed of two domains of predominantly β-sheet structure with the second domain inserted between the first and second half of the first domain (Figs. 1f, g and 2a, b). In the PorV complex the polypeptide sequences connecting the termini of the first cap domain to the barrel fold together to create another split-beta domain that forms a step-like structure running down the inside of the SprA barrel (Fig. 2a, b and Fig. 3a). This Step

domain shows high surface sequence conservation (Fig. 3c) indicating that it may participate in a functional interaction with a protein not present in our purified SprA complexes. The equivalent EM density is not well-defined in the Plug complex. With the exception of the Step structure, the inside of the SprA barrel is empty (Fig. 2d, Supplementary Video 3) resulting in an internal solvent-filled pore of approximately 70 Å in diameter (measured Cα to Cα)(Fig. 3a and Extended Data Fig. 3b). A pore of this size would be large enough to permit the passage of the folded substrates of the T9SS[20–22]. A lateral opening in the wall of the SprA barrel links the barrel interior to the extracellular membrane surface (Fig. 1g, Extended Data Fig. 3b, Supplementary Videos 3, 4). In the PorV complex the lateral opening is completely blocked by PorV which binds across its exterior face (Fig. 1g). In the Plug complex access to the lateral opening is unobstructed, but the periplasmic end of the barrel is now occluded by the Plug protein. Thus, the SprA cavity is opened to opposite sides of the membrane in the two complexes and neither complex provides an unimpeded pathway across the outer membrane. The size of the lateral opening is larger (~45 Å diameter) in the Plug complex than the PorV complex due to increased disorder in the loops surrounding the opening in the absence of bound PorV (Extended Data Fig. 3b).

The 36-strand barrel of SprA is the largest single polypeptide transmembrane β-barrel identified to date[19], far exceeding the size of the 26-strand lipopolysaccharide transporter LptD (Fig. 3d). Indeed, the LptD protein has an internal pore that is 2.5 times smaller in cross-sectional area than that of SprA[23,24]. The secretin family of outer membrane proteins form a similar size channel to SprA, but are constructed from symmetric, higher-order, oligomers of small subunits rather than a single asymmetric polypeptide. For example, the Type II Secretion System secretin is a 60-stranded barrel built from 15 copies of a ~40 kDa GspD subunit[25] (Fig. 3d). Intriguingly, the outer membrane curli secretion channel formed from 9 CsgG proteins has the same number of β-strands as SprA but has a substantially narrower pore[26] (Fig. 3d).

Single polypeptide outer membrane β-barrels are inserted into the membrane by the Bam machinery[27]. If SprA also uses this machinery, it would be the only known Bam-integrated β-barrel that possesses large folded extracellular domains. The size and complexity of the SprA fold makes it difficult to predict how insertion of the barrel and folding of the extracellular domains are coordinated, although it is possible that the folded domains are individually exported through the SprA pore once assembly of the barrel is completed.

Structural analysis of SprA partner proteins

Of the three proteins that co-purify with SprA, PPI is the only one that is present in both the PorV and Plug complex structures (Fig. 1g). Surprisingly for a protein with peptidyl-prolyl *cis-trans* isomerase activity, the PPI protein is located on the extracellular side of the membrane. PPI contacts SprA through two insertions near the C-terminus of the SprA barrel (Fig. 1f and Fig. 2a). These insertions overhang the barrel edge and form fingers that ‘grab’ PPI (Fig. 1f and Fig. 2a). It is notable that one of the insertions occurs in the middle of a barrel strand (β-strand [28]), splitting the strand in two and burying the insertion junction within the membrane bilayer (Fig. 2c). To the best of our knowledge this is the first time that insertion within a strand has been observed in an outer membrane β-barrel protein. Binding

of PPI to the overhang domain is mediated, in part, by insertion of a Pro-containing SprA surface loop into the PPI active site[28] (Fig. 2d). The lipidated N-terminus of PPI is not visible in the EM density. However, the PPI molecule is appropriately oriented to allow membrane insertion of the lipid anchor.

In the PorV complex the PorV protein binds across the lateral opening of SprA on the opposite side of the molecule to PPI (Fig. 1g). The packing interactions between PorV and the surface of SprA around the lateral opening are extensive and conserved (Fig. 3c). PorV is a member of the FadL family of 14-strand β-barrel outer membrane porins (Fig. 3b, Extended Data Fig. 3a)[29]. As in other FadL family members, the pore of PorV is plugged by the N-terminal region of the protein (Fig. 3b). In previously characterized FadL family members, barrel strand 3 kinks inwards to sit over an N-terminal `hatch' domain located within the periplasmic end of the barrel pore. However, in PorV the N-terminal region of the protein fills the pore and strands 3 and 4 bend outwards from the PorV barrel axis with their inter-strand loop penetrating the SprA barrel interior through the lateral opening (Fig. 1g, Supplementary Video 3). The PorV barrel is tilted by 25° relative to the SprA barrel (Extended Data Fig. 3c). From the positions of the belts of aromatic residues on the surface of PorV that would normally lie at the membrane polar–apolar interfaces (Extended Data Fig. 3c), we deduce that PorV adopts a more vertical position in the membrane bilayer when not in complex with SprA.

In the Plug complex structure, the disc-shaped Plug protein is inserted into the periplasmic end of the SprA barrel forming a tight seal between the barrel wall and the Plug rim (Fig. 1g and Supplementary Video 4). The interaction between SprA and the Plug is mediated solely through the Plug rim. Surface sequence conservation on the Plug is restricted to this contact interface (Fig. 3c) suggesting that the Plug has no other functional interactions. The location of the Plug protein in the Plug complex of SprA is sterically incompatible with the position of the Step domain seen in the PorV complex, explaining why the EM density for the Step domain is relocated and disordered in the Plug complex relative to the PorV complex.

A comparison of the two SprA complex structures shows that the cross-sectional shape of the SprA barrel changes from kidney-like in the PorV complex to almost circular in the Plug complex (Fig. 3a, Extended Data Fig. 3b, and Supplementary Video 5). The Plug protein has perfect shape complementarity with the circular conformer of the barrel but would be unable to fit within the narrower kidney-shaped conformer. By contrast, the binding site for PorV is formed by the concave exterior surface of the kidney-shaped conformer of the SprA barrel which does not exist in the circular conformer. Thus, in each of the two SprA complex structures the conformation of the barrel is intimately linked to the interaction SprA makes with its partner protein, and binding of PorV and the Plug protein to SprA is mutually exclusive. There are no significant changes in the folded extracellular domains or PPI between the PorV- and Plug complexes (Supplementary Video 5). Consequently, our structures provide no evidence for any re-organisation of the extracellular domains of SprA during the transport process.

SprA partner protein function

The identification of the PPI and Plug proteins in the T9SS translocon complexes was unanticipated. We examined the role of these proteins in T9S by constructing corresponding *F. johnsoniae* deletion strains and comparing the effect on T9SS function with strains lacking either SprA or PorV. SprA was stably expressed in cells lacking any of the other three proteins found in the SprA complexes (Extended Data Fig. 4a). Thus, these three partner proteins are not required for SprA biogenesis. T9SS function was assessed by analysing the secreted proteome and by examining gliding motility which depends on T9SS-exported adhesins[8,9] (Fig. 4a-c, Extended Data Fig. 4b-d, Supplementary Video 1). In agreement with a previous report[9], we observed that the loss of PorV prevents the secretion of most T9SS substrates but still permits gliding motility. By contrast, neither the loss of the Plug protein nor the PPI subunit had a detectable effect on T9SS function. Thus, the T9SS has no absolute requirements for the Plug or PPI protein in the transport process. Instead, a consideration of our structural data suggests that the role of the Plug protein might be to prevent non-specific leakage of periplasmic contents through the SprA channel. We reasoned that this function of the Plug protein would be revealed in a strain lacking both PorV and Plug because this strain would not be able to control movement of molecules through SprA. In agreement with this expectation, we found that a *porV plug* double mutant became sensitive to vancomycin (Fig. 4d and Extended Data Fig. 4e), an antibiotic that is normally excluded from Gram-negative bacteria because it is too large to fit through the protein channels present in the outer membrane[30]. Importantly, vancomycin resistance is restored if *sprA* is also deleted, showing that SprA mediates the increased outer membrane permeability observed in the absence of PorV and Plug. Control experiments confirm that the *porV plug* double mutant retains native levels of the SprA protein and phenocopies the transport phenotype of a *porV* single mutant (Fig. 4a-c and Extended Data Fig. 4a-d). Removal of the Plug protein alone also led to vancomycin sensitivity (Fig. 4d and Extended Data Fig. 4e) suggesting that the extracellular end of the SprA pore is routinely opened during the normal operation of the translocon. Taken together, the vancomycin sensitivity experiments demonstrate that the SprA protein forms a large outer membrane channel and that the Plug protein has a role in preventing small molecule leakage through SprA.

Discussion

Our structural data show that SprA forms a water-filled conduit across the outer membrane that is large enough to allow the passage of folded proteins. The lateral position of the extracellular exit from this channel ensures that exported T9SS substrates are directed towards the membrane surface for subsequent modification by the Attachment Complex. Our structures show that the two ends of the transport pathway through SprA are sealed by the Plug protein and PorV but that binding of these partner proteins is mutually exclusive. These observations suggest a model for the T9SS translocon mechanism in which the two ends of the transport channel are alternately gated (Fig. 4e). In this model the PorV-containing state of the translocon allows uptake of substrates from the periplasm into the SprA channel while the Plug complex represents the translocon after substrate release. Since PorV is known to interact with T9SS substrate proteins[13], we hypothesise that the translocon recognises substrate proteins in the interior of the SprA barrel through interactions between

the substrate CTD and the portions of PorV that are accessible through the lateral opening. This interaction is proposed to trigger the release of the PorV-substrate complex from the translocon. Once the periplasmic end of the SprA pore is clear of substrate protein we suggest that the Plug protein seals the SprA channel until a PorV molecule is once more bound at the lateral opening. This mechanistic model leads to unidirectional transport of the substrate through the T9SS translocon.

Methods

No statistical methods were used to predetermine sample size. The experiments were not randomized and the investigators were not blinded to allocation during experiments and outcome assessment.

Bacterial strains and growth conditions

All strains and plasmids used in this work are listed in Extended Data Table 2. *F. johnsoniae* was routinely grown in Casitone Yeast Extract (CYE) medium[32] at 25 °C with shaking. For some studies the cells were cultured on Motility Medium[33] or PY2 medium[34] as described below. Where required, 100μg/ml erythromycin was included in the growth medium.

Genetic constructs

A suicide plasmid to introduce an in-frame unmarked deletion of *sprA* was produced as follows. A 2.5 kbp fragment corresponding to the first 57 bp of *sprA* together with the directly upstream region was amplified using primers FL199 and FL200. Similarly, a 2.5 kbp fragment corresponding to the last 72bp of *sprA* and the directly downstream region was amplified with primers FL201 and FL202. Finally, plasmid pYT313[35] was linearized by PCR amplification using FL203 and FL204. The three amplicons were then assembled by Gibson cloning resulting in plasmid pFL58. Suicide plasmids to construct in-frame deletions in *porV* (*fjoh_1555*), *fjoh_1759* (*plug*), and *fjoh_4997* (*ppi*) were constructed in an analogous way using the oligonucleotides specified in Supplementary Table 1.

To produce a strain in which a HaloTag is inserted between the signal peptide and mature region of SprA the following suicide plasmid was constructed. A 2.5 kbp fragment corresponding to the first 63bp of *sprA* and directly upstream region was amplified using primers FL217 and FL218. This fragment was inserted between the NcoI and SpeI sites of pGEM-T Easy to generate pFL56. A 2.7 kbp fragment covering nucleotides 55 to 2770 of *sprA* was amplified using primers FL219 and FL220. This fragment was inserted between the SpeI and SacI sites of pFL56 to generate pFL57. The HaloTag-coding sequence was amplified from plasmid pHTC HaloTag® CMV-neo using primers FL178 and FL227 and the resulting fragment was ligated between the BamHI and SpeI sites of pFL57, yielding pFL61. The *halotag*::s*prA* fusion sequence from pFL61 was then introduced into pYT313 using Gibson assembly to generate pFL64. The suicide plasmid used to produce a strain with a Twin-Strep tag between the signal peptide and mature region of SprA was constructed by replacing the HaloTag-coding sequence in pFL61 by a Twin-Strep tag-coding sequence using Q5 site-directed mutagenesis (New England Biolabs) with primers FL221 and FL222,

yielding pFL66. The resulting fusion sequence was then introduced into pYT313 using Gibson assembly to generate pFL67.

Suicide plasmids were introduced into the appropriate *F. johnsoniae* background strain by biparental mating using *E. coli* S17-1[36] as donor strain, as previously described[32], and erythromycin resistance used to select cells with chromosomally integrated plasmid. One of the resulting clones was grown overnight in CYE without antibiotics to allow for loss of the plasmid backbone and then plated on CYE agar containing 5 % sucrose. Sucrose-resistant colonies were screened by PCR for the presence of the desired chromosomal modification and then verified by sequencing.

Purification of SprA complexes

F. johnsoniae Fl_012 was cultured aerobically at 25 °C for 22 h in 10 l of CYE medium. Cells were harvested by centrifugation at 6,000xg for 25 min and stored at -20 °C until further use. All purification steps were carried out at 4 °C. Cell pellets were resuspended in buffer W (100 mM Tris-HCl, pH 8, 150 mM NaCl, 1 mM EDTA) containing 30 μg/ml DNase I, 400 μg/ml lysozyme and 1 mM PMSF at a ratio of 7.5 ml of buffer/1 g of cell pellet. Cells were incubated on ice for 30 min before being lysed by two passages through a TS series 1.1 kW cell disruptor (Constant System Ltd) at 30,000 PSI. Unbroken cells were removed by centrifugation at 10,000xg for 10 min. The supernatant was recovered and total membranes were collected by centrifugation at 150,000xg for 75 min. Membranes were resuspended in buffer W to a protein concentration of 6.5 mg/ml and solubilized by incubation with 1 % (w/v) Lauryl Maltose Neopentyl Glycol (LMNG)(Anatrace) for 2 hours. Insoluble material was removed by centrifugation at 150,000xg for 60 min. The supernatant was then circulated through a StrepTrap HP column (GE Healthcare) overnight. The column was washed with 15 column volumes (CV) of buffer W containing 0.01% LMNG (buffer WD) and bound proteins were eluted with 6 CV buffer WD containing 2.5 mM desthiobiotin. The eluate was concentrated to 500 μl using a 100 kDa molecular weight cutoff (MWCO) Amicon ultra-15 centrifugal filter unit, and injected onto a Superose 6 Increase 10/300 GL column (GE Healthcare) previously equilibrated in buffer WD. Peak fractions were collected and concentrated using a 100kDa MWCO Vivaspin 500 column.

Cryo-EM sample preparation and data collection

The samples imaged were purified SprA at A_{280nm} = 1.0 in buffer WD, purified SprA at A_{280nm} = 2.0 in buffer WD with 1.5 mM fluorinated Fos-Choline 8 (Anatrace), or purified SprA at A_{280nm} = 2.3 in buffer WD with 0.7 mM fluorinated octyl maltoside (Anatrace). 4 ul of each sample was applied onto glow-discharged holey carbon coated grids (Quantifoil 300 mesh, Au R1.2/1.3), adsorbed for 10 s, blotted for 2 s at 100 % humidity at 4 °C and plunge frozen in liquid ethane using a Vitrobot Mark IV (FEI).

Data were collected in counting mode on a Titan Krios G3 (FEI) operating at 300 kV with a GIF energy filter (Gatan) and K2 Summit detector (Gatan). Datasets were collected for each purified sample at a sampling of 0.85 Å/pixel, 6.5 e-/Å/s, 8 s exposure, total dose 52 e-/$Å^2$, 20 fractions written totalling 14,553 movies. Motion correction and dose-weighting was performed with SIMPLE-unblur[37] and contrast transfer functions (CTFs) of the summed

micrographs were calculated using CTFFIND4[38]. Dose-weighted micrographs were subjected to picking using SIMPLE[37] and extraction with a 300 x 300 Å box in Relion 2.0[39], which was used for all further processing. Reference-free 2D classification was performed separately for each dataset. A low resolution initial model generated from the fluorinated octyl maltoside dataset was used as reference for 3D classification of all particles. Particles associated with PorV complex or Plug complex models were subjected to auto-refinement using a corresponding lowpass-filtered map. A final masked auto-refinement was carried out with the resulting models as references using 240,826 particles for the PorV complex or 118,090 particles for the Plug complex. Post-processing was carried using a soft mask with B-factor of -155 $Å^2$ (PorV complex) or -157 $Å^2$ (Plug complex) and a calibrated pixel size of 0.82 Å/pixel. Gold standard Fourier shell correlations using the 0.143 criterion led to resolution estimates of 3.5 Å for the PorV complex and 3.7 Å for the Plug complex. Local resolution estimations were calculated within Relion 2.0.

The EM processing workflow is detailed schematically in Extended Data Fig. 5.

Model building and refinement

A backbone trace of the PorV complex was manually made using program COOT[38] in a 4.2 Å map with 2423 alpha carbons placed, more than the full length of SprA, implying other components of the system had been co-purified and imaged with the tagged SprA. Inspection of this model allowed identification of an unconnected domain at the periphery of the complex. A structure-based search of the PDB using PDBefold revealed this domain to be of the FKBP-prolyl peptide isomerase family of proteins (chain A of 5hua being the highest hit). Since a member of this family had been identified in the sample by proteomics, this portion of the trace was assumed to be Fjoh_4997 and sequence for this protein was docked using 5hua as a guide. A similar search with the small beta barrel domain established OmpG (4ctd) as the closest structural homologue and confirmed assignment of N and C terminal strands within the barrel. Incorporation of additional particles and further refinement of the volume yielded a 3.5 Å map with clear sidechain densities throughout the volume. The sidechains decorating the small barrel structure were consistent with the sequence of the PorV homologue (Fjoh_1555) identified in the sample by proteomics.

The Plug complex was built using the PorV complex (with the PorV barrel removed) as a starting model, which left a large ordered portion of density unoccupied. As for PPI and PorV components, an alpha carbon trace was built into this density and PDBefold identified a protein of unknown function (4r7f, a hypothetical protein from *Parabacteriodes merdae*) as sharing the same fold.

Multiple rounds of rebuilding (in both the globally sharpened and model-based sharpened maps) and real-space refinement in Phenix[40] using secondary structure, rotamer and Ramachandran restraints yielded the final models described in Table 1. The PorV complex was used as a reference model to provide additional restraints for refinement of the Plug complex.

Protein models have been deposited in the PDB with accession numbers 6h3i and 6h3j, and EM volumes in the EMDB with accession numbers EMD-0133 and EMD-0134. Amino acid

residues are numbered relative to the start of the corresponding native precursor protein. See Extended Data Table 1 for cryo-EM data collection, refinement and validation statistics. Protein structure figures were prepared using Pymol Version 2.0 (Schrödinger, LLC) and ChimeraX[41].

Immunoblotting

For whole cell immunoblots strains were cultured to mid-log phase (OD_{600} = 0.3-0.4) in Motility Medium. Proteins were then transferred onto polyvinylidene difluoride (PVDF) membranes and probed with primary antibodies (anti-StrepTag [34850, Qiagen], anti-HaloTag [G921A, Promega], or anti-ChiA) followed by appropriate secondary antibodies (anti-mouse [A4416, Merck], anti-rabbit [31462, Pierce]). ChiA antibodies were raised against urea-solubilized inclusion bodies of a recombinant protein (expressed from plasmid pFL53) corresponding to the N-terminal glycoside hydrolase domain of ChiA.

Proteomics

Gel bands were cut and subjected to in-gel trypsin digestion as previously described[42]. The resulting digests were analyzed by a nano-flow reversed-phase liquid chromatograph coupled to a Q Exactive Hybrid Quadrupole-Orbitrap mass spectrometer (Thermo Fisher Scientific). The digests were loaded on a C18 PepMap100 pre-column (inner diameter 300 μm × 5 mm, 3 μm C18 beads; Thermo Fisher Scientific) and separated on a 50 cm reversed-phase C18 column (inner diameter 75 μm, 2 μm C18 beads) using a linear gradient from 10 to 35 % of B for 30 min at a flow rate of 200 nl/min (A: 0.1 % formic acid, B: 0.1 % formic acid in acetonitrile). All data were acquired in a data-dependent mode, automatically switching from MS to collision-induced dissociation MS/MS on the top 10 most abundant ions with a precursor scan range of 350–2000 m/z. MS spectra were acquired at a resolution of 70,000 and MS/MS scans at 17,500. Dynamic exclusion was enabled with an exclusion duration of 5 s and charge exclusion was applied to unassigned, and mono-charged ions. Raw data files were processed for protein identification using MaxQuant, version 1.5.0.35, integrated with the Andromeda search engine as described previously[43–45]. The MS/MS spectra were searched against the *Flavobacterium johnsoniae* UW101 Uniprot database. Precursor mass tolerance was set to 20 ppm and MS/MS tolerance to 0.05 Da. Enzyme specificity was set to trypsin with a maximum of two missed cleavages. False discovery rate for protein and peptide spectral matches was set at 0.01.

To analyse the secreted proteome strains were grown to late-log phase in CYE medium and a 10 ml sample of the culture collected when the OD_{600} reached 4.5. Cells were removed by centrifugation at 9,000xg for 25 min and the supernatant then filtered using a 0.22 μm syringe filter unit (Millipore). The supernatant was further clarified by centrifugation at 150,000xg for 75 min. The resulting supernatant was concentrated to 350 μl using a 10 kDa molecular weight cutoff (MWCO) Amicon ultra-15 centrifugal filter unit. 25 μl of this secreted protein fraction was subject to SDS-PAGE. Proteins were visualized by Coomassie Blue staining and the whole gel lane was excised for mass spectrometry analysis.

Europe PMC Funders Author Manuscripts

Measurement of gliding motility on agar

Strains were grown overnight in PY2 medium, washed once with fresh medium, and resuspended in PY2 medium to OD_{600} = 0.1. 2 µl of cell suspension were then spotted on to PY2 agar plates and incubated at 25 °C for 24 h. Colonies were imaged using a Zeiss AXIO Zoom.V16 microscope equipped with a Zeiss AxioCAM MRm CCD camera and the Zeiss software (ZenPro 2012, version 1.1.1.0).

Microscopic observation of live cells

Cells for bright field microscopic observation of gliding motility on glass were grown overnight in Motility Medium, inoculated into fresh medium at a 1:40 dilution, and grown for 5 h at 25 °C and at 50 rpm to a final OD_{600} = 0.3-0.4. An aliquot of the cell culture was introduced into a tunnel slide, incubated for 5 min, washed twice with 100 µl Motility Medium and imaged.

For fluorescence imaging cells were prepared in PY2 medium to reduce background fluorescence. Cells were cultured as above but in PY2 medium and to an OD_{600} = 0.1-0.2. The HaloTag-SprA fusion was labelled by mixing 1 ml of this culture with 1 µl of a 10 µM stock solution of Janelia Fluor 646 HaloTag ligand[46] in dimethyl sulfoxide (DMSO) and incubating for a further 20 min at 25 °C and 50 rpm. Cells were harvested by centrifugation, washed three times with PY2 medium, and resuspended in 50 µl of PY2 medium. To observe immobilized cells, 1 µl of cell suspension was spotted on a 1 % agarose pad containing 50 % PY2 medium. The spot was allowed to dry for 1 min and the cells were overlaid with a coverslip before imaging. To observe gliding motility on glass an aliquot of the cell culture was introduced into a tunnel slide, incubated for 5 min, washed twice with 100 µl PY2 medium, and imaged.

All bright field and fluorescence images were acquired at 25 °C using a Nanoimager (Oxford Nanoimaging) equipped with a 640nm 1W DPSS laser. Optical magnification was provided by a 100x oil-immersion objective (Olympus, numerical aperture (NA) 1.4) and images were acquired using an ORCA-Flash4.0 V3 CMOS camera (Hamamatsu). All fluorescence images were collected at 15% laser power. Measurement of the number of fluorescent SprA foci per cell was carried out using the ImageJ[47] plugin ThunderSTORM[48] with the following camera settings: pixel size, 117 nm; photoelectrons per A/D count, 0.46; base level, 100; and otherwise default settings. Bleaching analysis of SprA foci was carried out using the Nanoimager software.

Vancomycin sensitivity assay

Strains were grown to mid-log phase (OD_{600} = 0.3-0.4) in Motility Medium. Cultures were then diluted to an OD_{600} = 0.1 and 100 µl of the cell suspension used to inoculate CYE agar. Plates were allowed to dry for 20 min at room temperature. Filter paper discs containing 100 µg vancomycin hydrochloride (Merck) dissolved in DMSO were then placed on top of the agar. Inhibition zones were imaged after 48 h of incubation at 25 °C using a G:box ChemiXX6 (Syngene) equipped with a Synaptics 6MP camera and running GeneSys version 1.5.40 software.

Extended Data

Europe PMC Funders Author Manuscripts

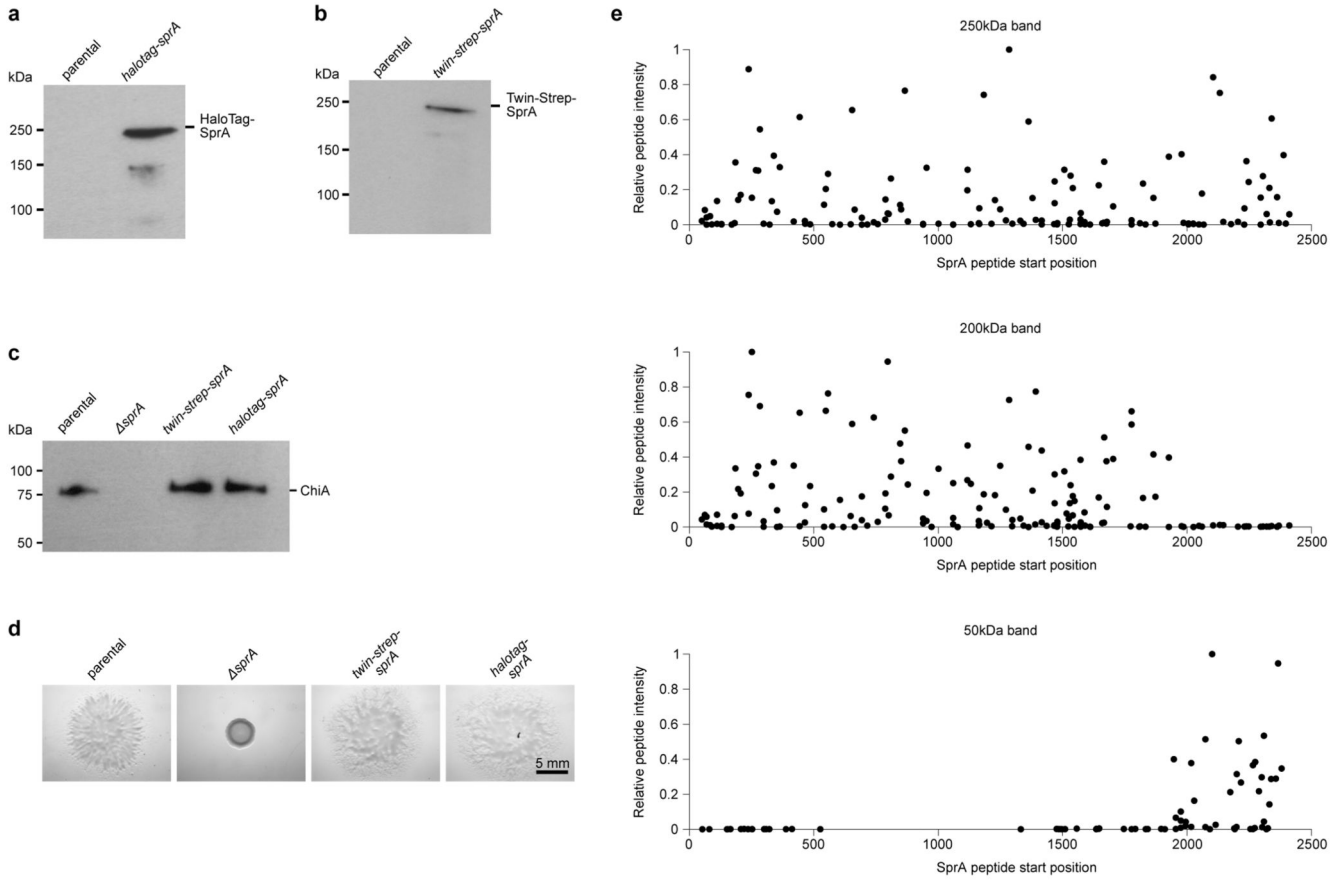

Extended Data Fig. 1. Phenotypic analysis of strains expressing Halotag and Twin-Strep-SprA fusion proteins.

a,b, Immunoblot analysis of (**a**) HaloTag-SprA and (**b**) Twin-Strep-SprA expression in whole cell lysates. Similar data were obtained for three biological repeats. **c,** Immunoblot detection of the T9SS-dependent chitinase ChiA levels in culture supernatants. Similar data were obtained for three biological repeats. **d,** T9SS-dependent spreading (gliding) morphology of colonies on agar. Scale bar, 5 mm. Similar data were obtained for three biological repeats. **e,** Peptide mass spectrometry of the three highest molecular mass bands in Fig. 1d. Intensity values are normalized to the most abundant SprA peptide detected for each band. Peptide numbering is from the N-terminus of the native SprA precursor sequence. For immunoblot source data see Supplementary Fig. 1.

Europe PMC Funders Author Manuscripts

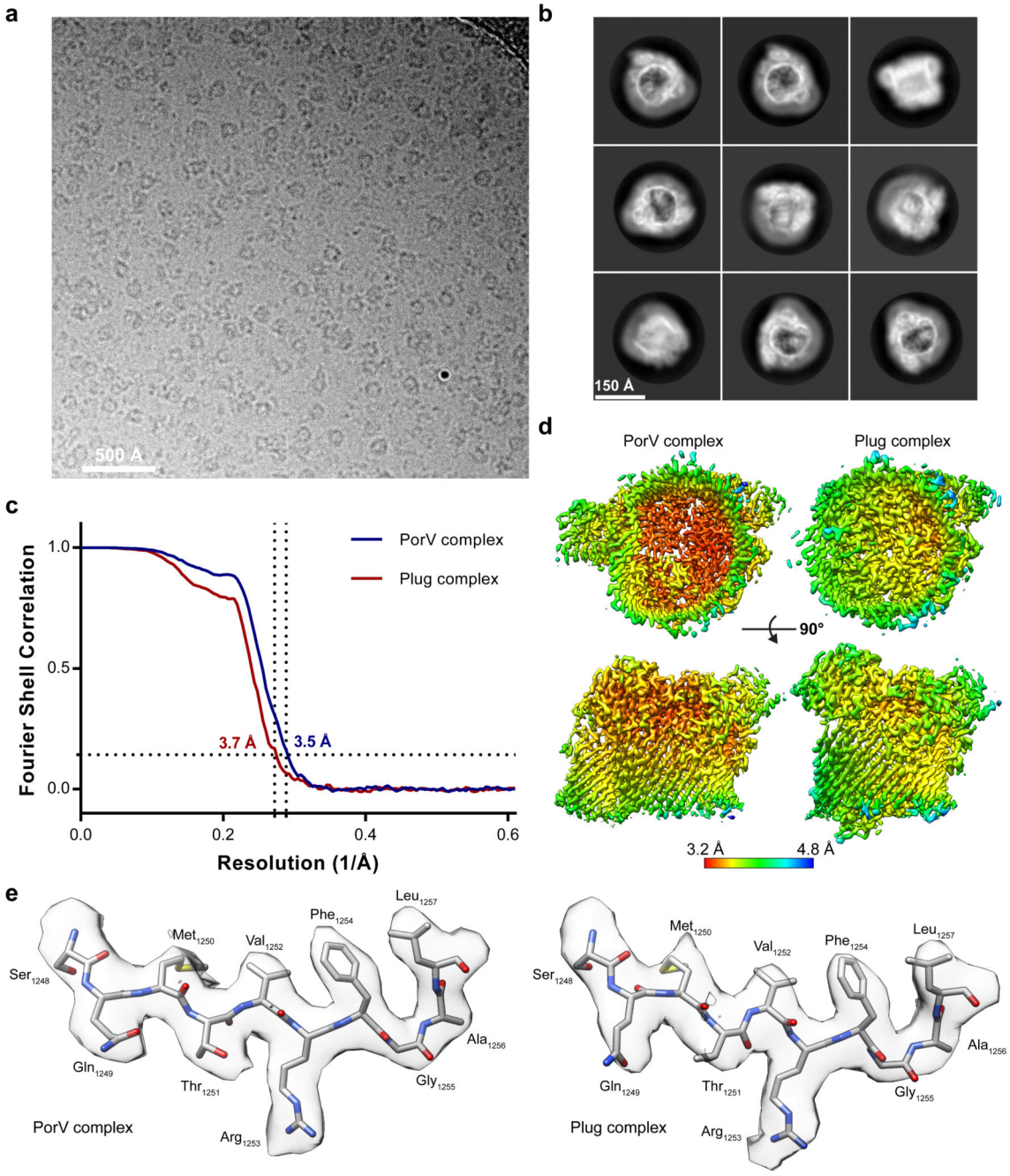

Extended Data Fig. 2. Experimental quality and resolution estimation of SprA complexes.

a, Representative micrograph of SprA complexes. **b,** Selected reference-free 2D class averages. **c,** Gold-standard FSC curve of the final map calculated using a soft-edged mask. **d,** Local resolution estimates of the final maps. **e,** Representative density for SprA in the PorV complex (left) and Plug complex (right).

Europe PMC Funders Author Manuscripts

Europe PMC Funders Author Manuscripts

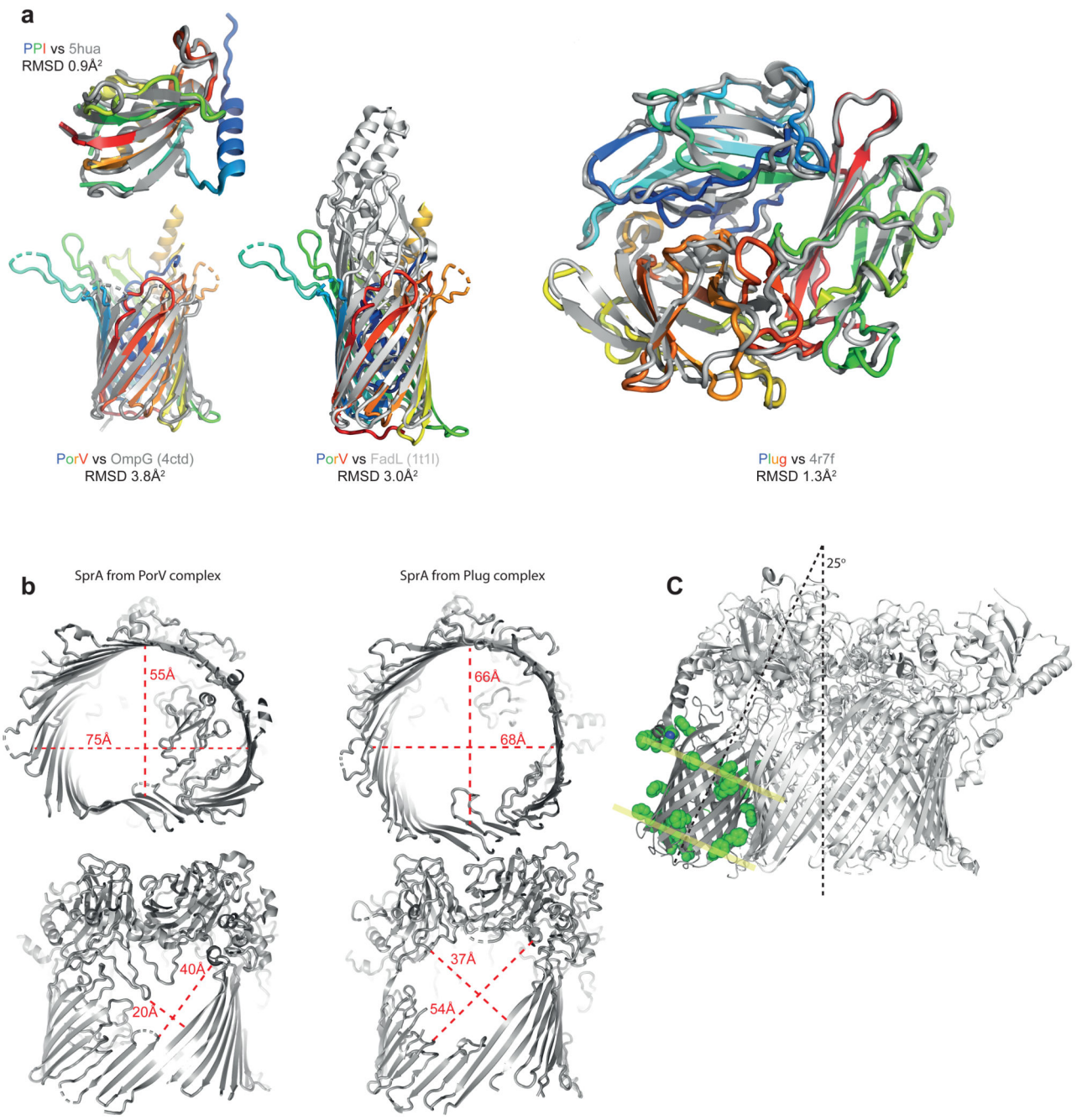

Extended Data Fig. 3. Structural analysis of the SprA complex components.

a, Structural alignment of SprA-bound proteins against the homology models used in initial sequence docking. **b,** Access routes to the SprA pore viewed (Top) from the periplasm or (Bottom) towards the lateral opening. In the PorV complex two loops involved in coordinating PorV occlude the lateral opening. The step domain is poorly ordered in the Plug complex. For clarity, PorV, Plug, and PPI are not shown. **c,** The PorV barrel is tilted relative to the SprA barrel. Aromatic residues on the surface of PorV are shown in green spacefill.

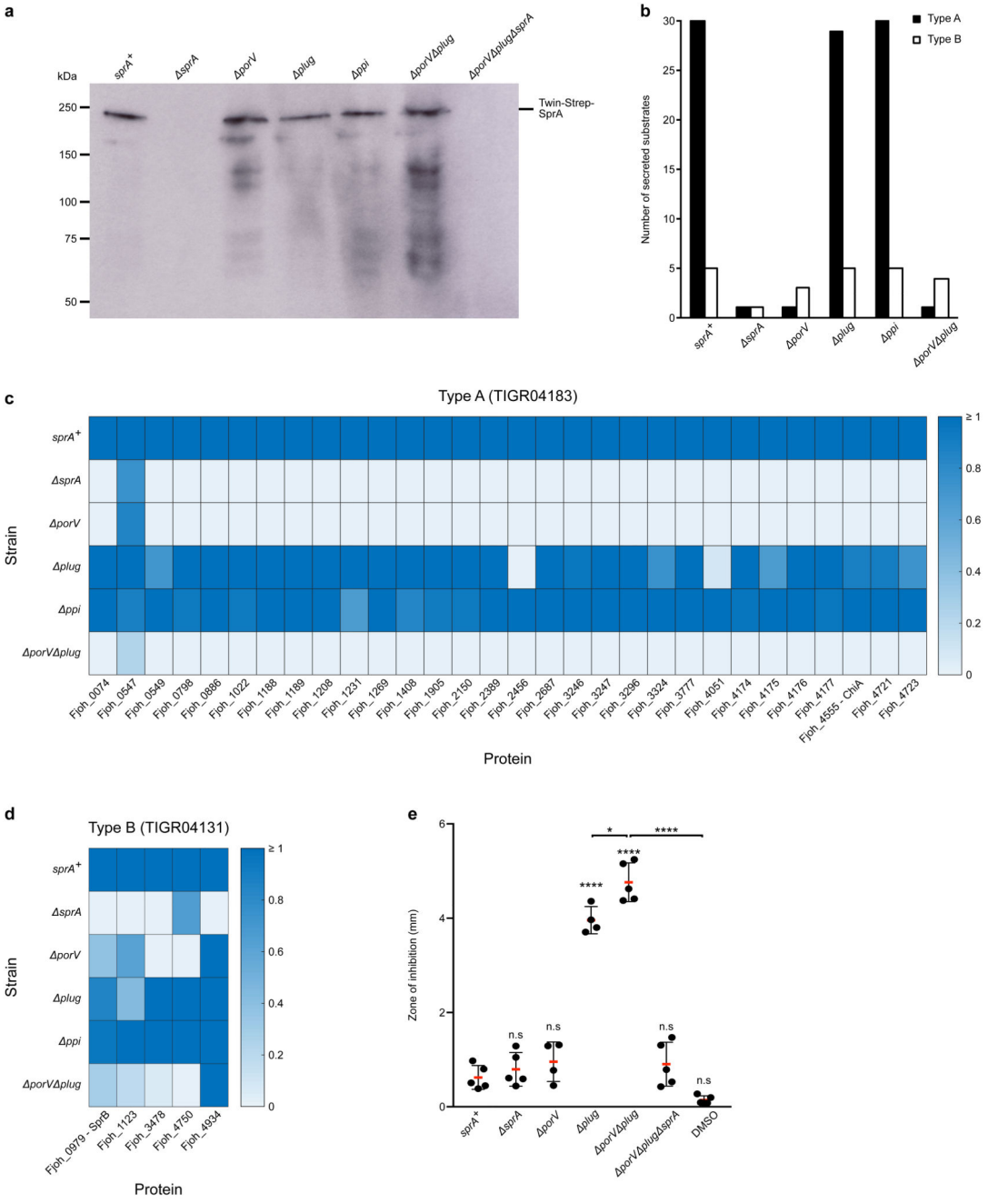

Extended Data Fig. 4. Phenotypes of SprA partner deletion strains.

a, Immunoblot analysis of Twin-Strep-SprA levels in whole cell lysates. Similar data were obtained for three biological repeats. For immunoblot source data see Supplementary Fig. 1. **b,** Quantification by liquid chromatography–mass spectrometry of T9SS substrates detected in cell culture supernatants according to CTD type. A detection threshold of >1% of the protein abundance in the *sprA*$^{+}$ parental strain was applied. **c, d,** Heat map representation of secreted T9SS substrates from **b** with either (**c**) type A CTDs or (**d**) type B CTDs. Protein intensities for each protein are normalised to the level detected in the *sprA*$^{+}$ parental strain.

Europe PMC Funders Author Manuscripts

e, Measurement of vancomycin inhibition zones in a disc diffusion assay. The mean radius of inhibition (red bar) is measured from the disc edge. Error bars represent 1SD (n=4 for Δ*porV* and Δ*plug*; n=5 for other strains) and statistical significance is indicated above each measurement set from a one-way ANOVA with post-hoc Dunnett's test using *sprA*$^{+}$ as control group (n.s. = not significant, **** = $p < 0.0001$). Other comparisons (bracketed) use two tailed unpaired t tests *, $p = 0.0134$; ****, $p < 0.0001$). A control for the DMSO solvent used to dissolve the vancomycin is shown. **a-e,** All *sprA*$^{+}$ strains are expressing the Twin-Strep-SprA fusion.

Europe PMC Funders Author Manuscripts

Europe PMC Funders Author Manuscripts

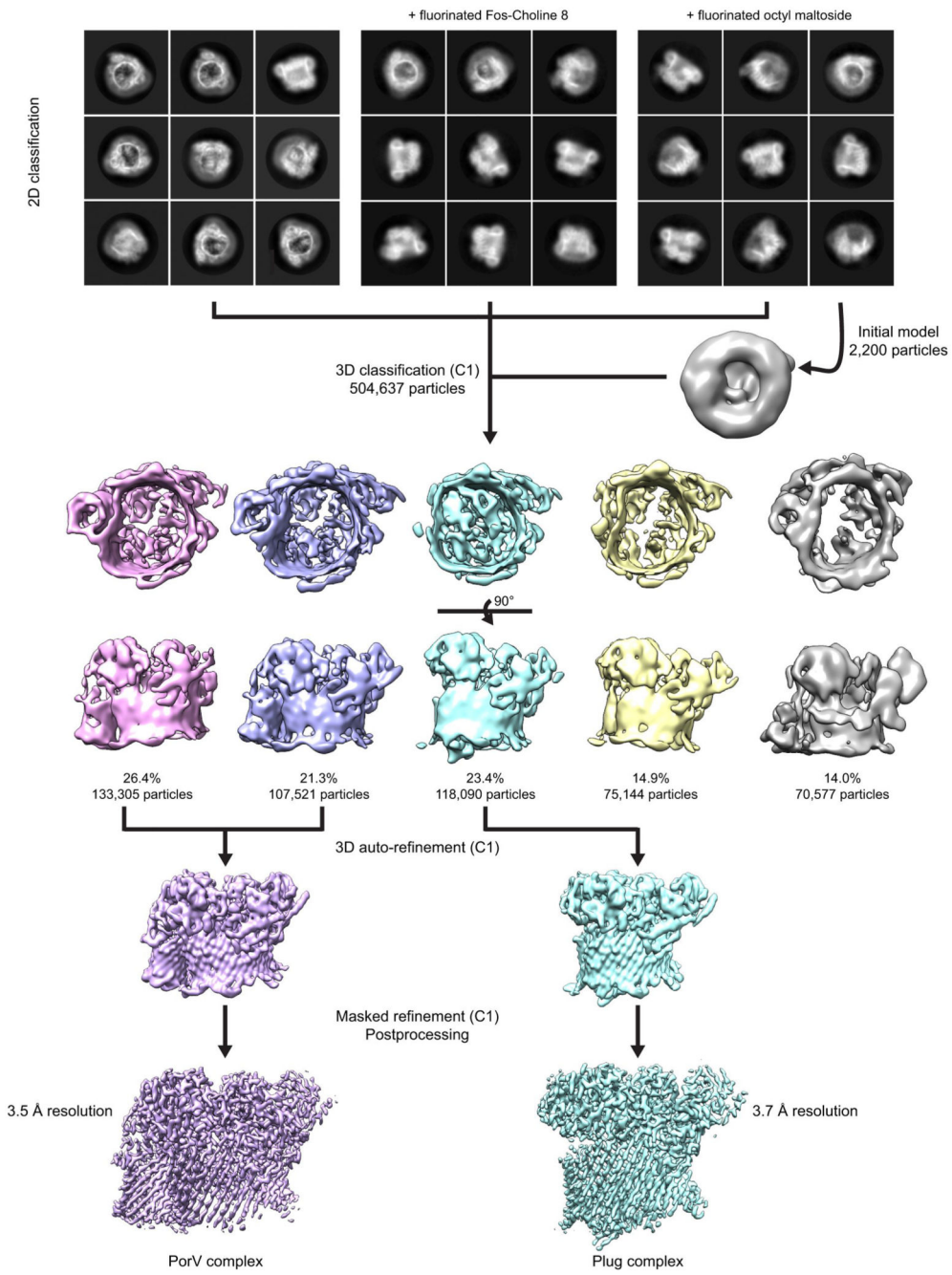

Extended Data Fig. 5. Single-particle cryo-EM image processing workflow for the SprA complexes.

Cryo-EM data sets of SprA complexes in LMNG, in the presence or absence of fluorinated detergents, were combined following 2D classification and subjected to 3D classification against a low resolution model generated from the fluorinated octyl-maltoside dataset. Particle images corresponding to the PorV complex or Plug complex were then independently refined. A soft mask, generated from these maps, was then used to perform masked refinement against the same particle images, resulting in global map resolutions of 3.5 Å for the PorV complex and 3.7 Å for the Plug complex.

Extended Data Table 1

Cryo-EM data collection, refinement and validation statistics.

	PorV complex (EMD-0133) (PDB 6h3i)	Plug complex (EMD-0134) (PDB 6h3j)
Data collection and processing		
Magnification	165,000	
Voltage (kV)	300	
Electron exposure (e–/Å^2)	52	
Defocus range (μm)	1.0-3.0	
Pixel size (Å)	0.82	
Symmetry imposed	C1	
Initial particle images (no.)	504,637	504,637
Final particle images (no.)	240,826	118,090
Map resolution (Å)	3.5	3.7
FSC threshold	0.143	0.143
Map resolution range (Å)	3.3-5.0	3.4-4.7
Refinement		
Initial model used (PDB code)	none	PorV complex + 4r7f (chain C)
Model resolution (Å)	3.5	3.7
FSC threshold	0.143	0.143
Model resolution range (Å)	3.3-5.0	3.4-4.7
Map sharpening *B* factor (Å^2)	-155	-157
Model composition		
Non-hydrogen atoms	20,546	20,089
Protein residues	2,597	2,511
	(SprA 2,124; FJOH_4997 128; FJOH_1555 345)	(SprA 1,988; FJOH_4997 126; FJOH_1749 397)
Ligands	0	0
B factors (Å^2)	50	58
Protein	(SprA 46; FJOH_4997 73; FJOH_1555 67)	(SprA 57; FJOH_4997 85; FJOH_1759 51)
R.m.s deviations		
Bond lengths (Å)	0.009	0.007
Bond angles (°)	0.9	0.8
Validation		
MolProbity score	2.2	2.3
Clashscore	8.6	9.5
Poor rotamers (%)	0.4	0.05
Ramachandran plot		

	PorV complex (EMD-0133) (PDB 6h3i)	Plug complex (EMD-0134) (PDB 6h3j)
Favored (%)	78	76
Allowed (%)	21	24
Disallowed (%)	0.2	0.04

PorV-complex, model to map fit CC_mask=0.84
Plug-complex, model to map fit CC_mask=0.83

Extended Data Table 2
Bacterial strains and plasmids used in this study.

Strain	Genotype	Reference
E. coli		
S17-1	*pro, res*$^{-}$ *hsdR17 (rK*$^{-}$ *mK*$^{+}$*) recA*$^{-}$*, RP4-2-Tc::Mu-Km::Tn7*, Tp^{r}	35
F. johnsoniae		
UW101		49
Fl_004	UW101 Δ*sprA*	This study
Fl_012	UW101 *twin-strep-tag::sprA*	This study
Fl_016	UW101 *halotag::sprA*	This study
Fl_036	Fl_012 Δ*porV (fjoh_1555)*	This study
Fl_038	Fl_012 Δ*fjoh_1759 (plug)*	This study
Fl_040	Fl_012 Δ*fjoh_4997 (ppi)*	This study
Fl_058	Fl_012 Δ*porV (fjoh_1555) Δfjoh_1759 (plug)*	This study
Fl_068	Fl_012 Δ*porV (fjoh_1555) Δfjoh_1759 (plug)* Δ*sprA*	This study

Plasmid	Description[a]	Reference
pGEM-T Easy	General cloning vector; Ap^{r}	Promega
pYT313	*sacB*-containing mobilizable suicide vector; Ap^{r} (Em^{r})	34
pHTC HaloTag® CMV-neo	*Halotag*-containing plasmid	Promega
pET22b(+)	*E. coli* expression vector; Ap^{r}	Merck
pFL53	1.8-kbp fragment of *chiA* inserted between the NdeI and XhoI sites of pET22b(+)	This study
pFL56	2.5-kbp upstream of *sprA* (including the first 63bp of *sprA*) inserted between the NcoI and SpeI sites of pGEM-T Easy	This study
pFL57	2.7-kbp of *sprA* (bp 55 to 2770) inserted between the SpeI and SacI sites of pFL56	This study
pFL58	Construct used to delete *sprA*; contains 2.5-kbp upstream and 2.5-kbp downstream of *sprA* in pYT313	This study
pFL61	*halotag* inserted between the BamHI and SpeI sites of pFL57	This study
pFL64	*halotag::sprA* sequence from pFL61 in pYT313	This study
pFL66	*twin-strep-tag* inserted between the BamHI and SpeI sites of pFL57	This study
pFL67	*twin-strep-tag::sprA* sequence from pFL66 in pYT313	This study
pFL80	Construct used to delete *porV (fjoh_1555*); 2.5-kbp upstream and 2.5-kbp downstream of *porV* in pYT313	This study
pFL81	Construct used to delete *fjoh_1759 (plug);* 2.6-kbp upstream and 2.6-kbp downstream of *fjoh_1759* in pYT313	This study

pFL82	Construct used to delete *fjoh_4997 (ppi);* 2.6-kbp upstream and 2.7-kbp downstream of *fjoh_4997* in pYT313	This study

[a] Selection markers functional in *F. johnsoniae* are in brackets

Supplementary Material

Refer to Web version on PubMed Central for supplementary material.

Acknowledgements

We thank Mark McBride and Yongtao Zhu for providing reagents for the genetic manipulation of *F. johnsoniae*, and Abhishek Shrivastava and Howard Berg for advice on measuring gliding motility. We thank Luke Lavis for supplying the Janelia Fluor 646 HaloTag ligand and Sam Hickman for advice on fluorescence imaging. We acknowledge the use of Central Oxford Structural Microscopy and Imaging Centre (COSMIC), the Oxford Micron Advanced Imaging Facility, and the Oxford Advanced Proteomics Facility. We thank Oliver Meacock and Kevin Foster for providing additional imaging facilities. This work was supported by Wellcome Trust Investigator Awards 107929/Z/15/Z and 100298/Z/12/Z. COSMIC was supported by a Wellcome Trust Collaborative Award 201536/Z/16/Z, the Wolfson Foundation, a Royal Society Wolfson Refurbishment Grant, the John Fell Fund, and the EPA and Cephalosporin Trusts.

References

1. Veith PD, Glew MD, Gorasia DG, Reynolds EC. Type IX secretion: the generation of bacterial cell surface coatings involved in virulence, gliding motility and the degradation of complex biopolymers. Molecular microbiology. 2017; 106:35–53. DOI: 10.1111/mmi.13752 [PubMed: 28714554]
2. Lasica AM, Ksiazek M, Madej M, Potempa J. The Type IX Secretion System (T9SS): Highlights and Recent Insights into Its Structure and Function. Front Cell Infect Microbiol. 2017; 7:215.doi: 10.3389/fcimb.2017.00215 [PubMed: 28603700]
3. Li N, et al. The Type IX Secretion System Is Required for Virulence of the Fish Pathogen *Flavobacterium columnare*. Applied and environmental microbiology. 2017; 83doi: 10.1128/AEM.01769-17
4. Perez-Pascual D, et al. More Than Gliding: Involvement of GldD and GldG in the Virulence of *Flavobacterium psychrophilum*. Frontiers in microbiology. 2017; 8:2168.doi: 10.3389/fmicb.2017.02168 [PubMed: 29163446]
5. Shrivastava A, Roland T, Berg HC. The Screw-Like Movement of a Gliding Bacterium Is Powered by Spiral Motion of Cell-Surface Adhesins. Biophys J. 2016; 111:1008–1013. DOI: 10.1016/j.bpj.2016.07.043 [PubMed: 27602728]
6. McBride MJ, Nakane D. Flavobacterium gliding motility and the type IX secretion system. Current opinion in microbiology. 2015; 28:72–77. DOI: 10.1016/j.mib.2015.07.016 [PubMed: 26461123]
7. Shoji M, et al. Por secretion system-dependent secretion and glycosylation of *Porphyromonas gingivalis* hemin-binding protein 35. PloS one. 2011; 6:e21372.doi: 10.1371/journal.pone.0021372 [PubMed: 21731719]
8. Kulkarni SS, Zhu Y, Brendel CJ, McBride MJ. Diverse C-Terminal Sequences Involved in *Flavobacterium johnsoniae* Protein Secretion. Journal of bacteriology. 2017; 199doi: 10.1128/JB.00884-16
9. Kharade SS, McBride MJ. Flavobacterium johnsoniae PorV is required for secretion of a subset of proteins targeted to the type IX secretion system. Journal of bacteriology. 2015; 197:147–158. DOI: 10.1128/JB.02085-14 [PubMed: 25331433]
10. Heath JE, et al. PG1058 Is a Novel Multidomain Protein Component of the Bacterial Type IX Secretion System. PloS one. 2016; 11:e0164313.doi: 10.1371/journal.pone.0164313 [PubMed: 27711252]

11. Gorasia DG, et al. Structural Insights into the PorK and PorN Components of the *Porphyromonas gingivalis* Type IX Secretion System. Plos Pathog. 2016; 12:e1005820.doi: 10.1371/journal.ppat.1005820 [PubMed: 27509186]
12. Leone P, et al. Type IX secretion system PorM and gliding machinery GldM form arches spanning the periplasmic space. Nature communications. 2018; 9doi: 10.1038/s41467-017-02784-7
13. Glew MD, et al. PorV is an Outer Membrane Shuttle Protein for the Type IX Secretion System. Sci Rep. 2017; 7doi: 10.1038/s41598-017-09412-w
14. Glew MD, et al. PG0026 is the C-terminal signal peptidase of a novel secretion system of *Porphyromonas gingivalis*. The Journal of biological chemistry. 2012; 287:24605–24617. DOI: 10.1074/jbc.M112.369223 [PubMed: 22593568]
15. Gorasia DG, et al. *Porphyromonas gingivalis* Type IX Secretion Substrates Are Cleaved and Modified by a Sortase-Like Mechanism. Plos Pathog. 2015; 11:e1005152.doi: 10.1371/journal.ppat.1005152 [PubMed: 26340749]
16. Nelson SS, Glocka PP, Agarwal S, Grimm DP, McBride MJ. *Flavobacterium johnsoniae* SprA is a cell surface protein involved in gliding motility. Journal of bacteriology. 2007; 189:7145–7150. DOI: 10.1128/JB.00892-07 [PubMed: 17644580]
17. Saiki K, Konishi K. Identification of a *Porphyromonas gingivalis* novel protein sov required for the secretion of gingipains. Microbiol Immunol. 2007; 51:483–491. [PubMed: 17579257]
18. McBride MJ, Zhu Y. Gliding motility and Por secretion system genes are widespread among members of the phylum bacteroidetes. Journal of bacteriology. 2013; 195:270–278. DOI: 10.1128/JB.01962-12 [PubMed: 23123910]
19. Schiffrin B, Brockwell DJ, Radford SE. Outer membrane protein folding from an energy landscape perspective. BMC Biol. 2017; 15:123.doi: 10.1186/s12915-017-0464-5 [PubMed: 29268734]
20. Lasica AM, et al. Structural and functional probing of PorZ, an essential bacterial surface component of the type-IX secretion system of human oral-microbiomic *Porphyromonas gingivalis*. Sci Rep. 2016; 6doi: 10.1038/srep37708
21. Goulas T, et al. Structure and mechanism of a bacterial host-protein citrullinating virulence factor, *Porphyromonas gingivalis* peptidylarginine deiminase. Sci Rep. 2015; 5doi: 10.1038/srep11969
22. de Diego I, et al. *Porphyromonas gingivalis* virulence factor gingipain RgpB shows a unique zymogenic mechanism for cysteine peptidases. The Journal of biological chemistry. 2013; 288:14287–14296. DOI: 10.1074/jbc.M112.444927 [PubMed: 23558682]
23. Qiao S, Luo Q, Zhao Y, Zhang XC, Huang Y. Structural basis for lipopolysaccharide insertion in the bacterial outer membrane. Nature. 2014; 511:108–111. DOI: 10.1038/nature13484 [PubMed: 24990751]
24. Dong H, et al. Structural basis for outer membrane lipopolysaccharide insertion. Nature. 2014; 511:52–56. DOI: 10.1038/nature13464 [PubMed: 24990744]
25. Yan Z, Yin M, Xu D, Zhu Y, Li X. Structural insights into the secretin translocation channel in the type II secretion system. Nature structural & molecular biology. 2017; 24:177–183. DOI: 10.1038/nsmb.3350
26. Goyal P, et al. Structural and mechanistic insights into the bacterial amyloid secretion channel CsgG. Nature. 2014; 516:250–253. DOI: 10.1038/nature13768 [PubMed: 25219853]
27. Noinaj N, Gumbart JC, Buchanan SK. The beta-barrel assembly machinery in motion. Nature reviews. Microbiology. 2017; 15:197–204. DOI: 10.1038/nrmicro.2016.191 [PubMed: 28216659]
28. Quistgaard EM, et al. Molecular insights into substrate recognition and catalytic mechanism of the chaperone and FKBP peptidyl-prolyl isomerase SlyD. BMC Biol. 2016; 14:82.doi: 10.1186/s12915-016-0300-3 [PubMed: 27664121]
29. van den Berg B, Black PN, Clemons WM Jr, Rapoport TA. Crystal structure of the long-chain fatty acid transporter FadL. Science. 2004; 304:1506–1509. DOI: 10.1126/science.1097524 [PubMed: 15178802]
30. Zgurskaya HI, Lopez CA, Gnanakaran S. Permeability Barrier of Gram-Negative Cell Envelopes and Approaches To Bypass It. ACS Infect Dis. 2015; 1:512–522. DOI: 10.1021/acsinfecdis.5b00097 [PubMed: 26925460]

31. Ashkenazy H, et al. ConSurf 2016: an improved methodology to estimate and visualize evolutionary conservation in macromolecules. Nucleic Acids Res. 2016; 44:W344–350. DOI: 10.1093/nar/gkw408 [PubMed: 27166375]
32. McBride MJ, Kempf MJ. Development of techniques for the genetic manipulation of the gliding bacterium *Cytophaga johnsonae*. Journal of bacteriology. 1996; 178:583–590. [PubMed: 8550486]
33. Liu J, McBride MJ, Subramaniam S. Cell surface filaments of the gliding bacterium *Flavobacterium johnsoniae* revealed by cryo-electron tomography. Journal of bacteriology. 2007; 189:7503–7506. DOI: 10.1128/JB.00957-07 [PubMed: 17693495]
34. Agarwal S, Hunnicutt DW, McBride MJ. Cloning and characterization of the *Flavobacterium johnsoniae* (*Cytophaga johnsonae*) gliding motility gene, gldA. Proceedings of the National Academy of Sciences of the United States of America. 1997; 94:12139–12144. [PubMed: 9342376]
35. Zhu Y, et al. Genetic analyses unravel the crucial role of a horizontally acquired alginate lyase for brown algal biomass degradation by *Zobellia galactanivorans*. Environmental microbiology. 2017; 19:2164–2181. DOI: 10.1111/1462-2920.13699 [PubMed: 28205313]
36. Simon R, Priefer U, Puhler A. A Broad Host Range Mobilization System for In vivo Genetic Engineering - Transposon Mutagenesis in Gram-Negative Bacteria. Bio-Technol. 1983; 1:784–791. DOI: 10.1038/nbt1183-784
37. Reboul CF, Eager M, Elmlund D, Elmlund H. Single-particle cryo-EM-Improved ab initio 3D reconstruction with SIMPLE/PRIME. Protein Sci. 2018; 27:51–61. DOI: 10.1002/pro.3266 [PubMed: 28795512]
38. Brown A, et al. Tools for macromolecular model building and refinement into electron cryo-microscopy reconstructions. Acta crystallographica Section D, Biological crystallography. 2015; 71:136–153. DOI: 10.1107/S1399004714021683 [PubMed: 25615868]
39. Kimanius D, Forsberg BO, Scheres SH, Lindahl E. Accelerated cryo-EM structure determination with parallelisation using GPUs in RELION-2. Elife. 2016; 5doi: 10.7554/eLife.18722
40. Adams PD, et al. PHENIX: a comprehensive Python-based system for macromolecular structure solution. Acta crystallographica Section D, Biological crystallography. 2010; 66:213–221. DOI: 10.1107/S0907444909052925 [PubMed: 20124702]
41. Goddard TD, et al. UCSF ChimeraX: Meeting modern challenges in visualization and analysis. Protein Sci. 2018; 27:14–25. DOI: 10.1002/pro.3235 [PubMed: 28710774]
42. Shevchenko A, Tomas H, Havlis J, Olsen JV, Mann M. In-gel digestion for mass spectrometric characterization of proteins and proteomes. Nat Protoc. 2006; 1:2856–2860. DOI: 10.1038/nprot.2006.468 [PubMed: 17406544]
43. Cox J, Mann M. MaxQuant enables high peptide identification rates, individualized p.p.b.- range mass accuracies and proteome-wide protein quantification. Nat Biotechnol. 2008; 26:1367–1372. DOI: 10.1038/nbt.1511 [PubMed: 19029910]
44. Cox J, et al. Andromeda: a peptide search engine integrated into the MaxQuant environment. J Proteome Res. 2011; 10:1794–1805. DOI: 10.1021/pr101065j [PubMed: 21254760]
45. Tyanova S, et al. The Perseus computational platform for comprehensive analysis of (prote)omics data. Nat Methods. 2016; 13:731–740. DOI: 10.1038/nmeth.3901 [PubMed: 27348712]
46. Grimm JB, Brown TA, English BP, Lionnet T, Lavis LD. Synthesis of Janelia Fluor HaloTag and SNAP-Tag Ligands and Their Use in Cellular Imaging Experiments. Methods Mol Biol. 2017; 1663:179–188. DOI: 10.1007/978-1-4939-7265-4_15 [PubMed: 28924668]
47. Schneider CA, Rasband WS, Eliceiri KW. NIH Image to ImageJ: 25 years of image analysis. Nat Methods. 2012; 9:671–675. [PubMed: 22930834]
48. Ovesny M, Krizek P, Borkovec J, Svindrych Z, Hagen GM. ThunderSTORM: a comprehensive ImageJ plug-in for PALM and STORM data analysis and super-resolution imaging. Bioinformatics. 2014; 30:2389–2390. DOI: 10.1093/bioinformatics/btu202 [PubMed: 24771516]
49. McBride MJ, Braun TF. GldI is a lipoprotein that is required for *Flavobacterium johnsoniae* gliding motility and chitin utilization. Journal of bacteriology. 2004; 186:2295–2302. [PubMed: 15060031]

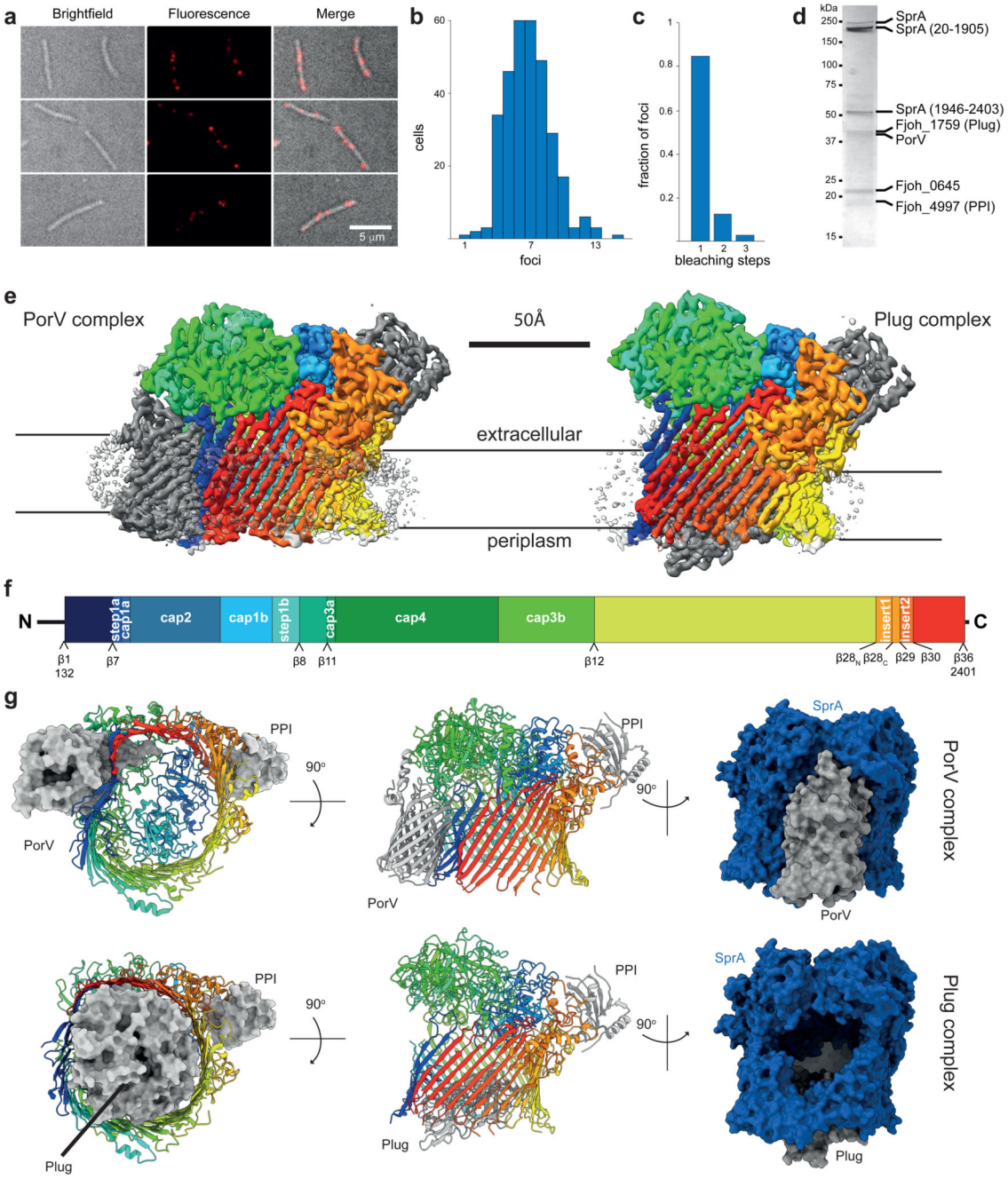

Fig. 1. Characterization of SprA.

a, Localization of fluorophore-labelled SprA in *F. johnsoniae* cells. Exemplar data from experiments repeated on three different cultures with similar results. **b, c,** Population distributions of (**b**) SprA foci per cell and (**c**) SprA molecules per focus (from 119 photobleaching traces). **d,** Coomassie-stained SDS-PAGE gel of affinity-purified SprA with band identities from peptide mass spectrometry. Fjoh_0645 is a biotin-containing contaminant protein that binds to the streptavidin affinity matrix. Similar data were obtained for three independent preparations. For gel source data see Supplementary Fig. 1. **e,** EM

Europe PMC Funders Author Manuscripts

density of the SprA complexes. Membrane position inferred from the location of the detergent micelles. **f,** Domain organisation of SprA. **g,** Overall structures of the SprA complexes. The same SprA domain colouring scheme is applied in **e**-**g** except in **g** far right panel (SprA-blue, PorV/Plug-grey).

Europe PMC Funders Author Manuscripts

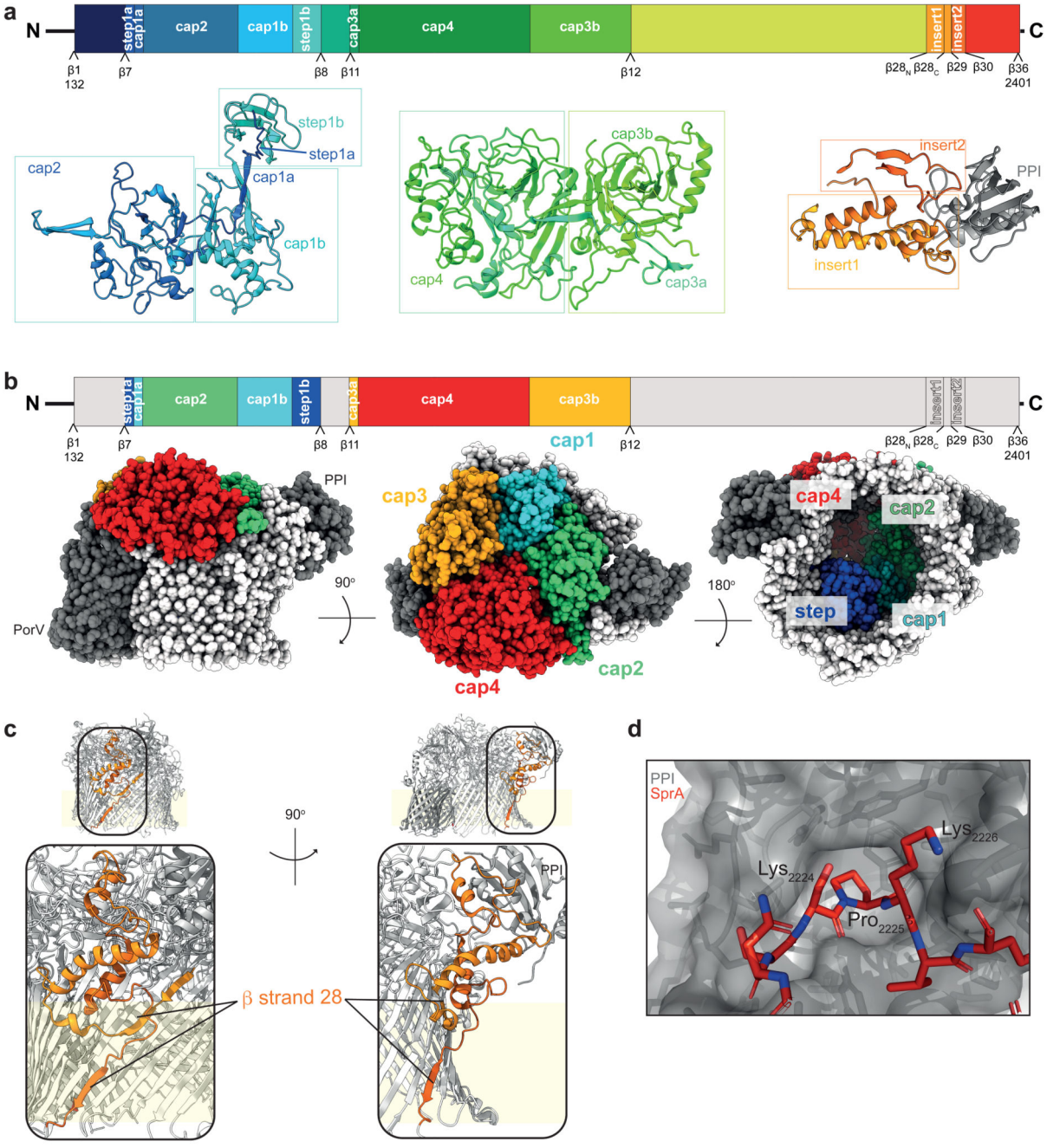

Fig. 2. Structural features of SprA extracellular domains.

a, Structures of the SprA step, cap domains, and inserts from the PorV complex. **b**, Locations of the cap and step domains in the PorV complex. **c,** Insert 1 is inserted within SprA β-strand 28. **d,** The PPI active site contains a proline-containing SprA surface loop (red).

Europe PMC Funders Author Manuscripts

Europe PMC Funders Author Manuscripts

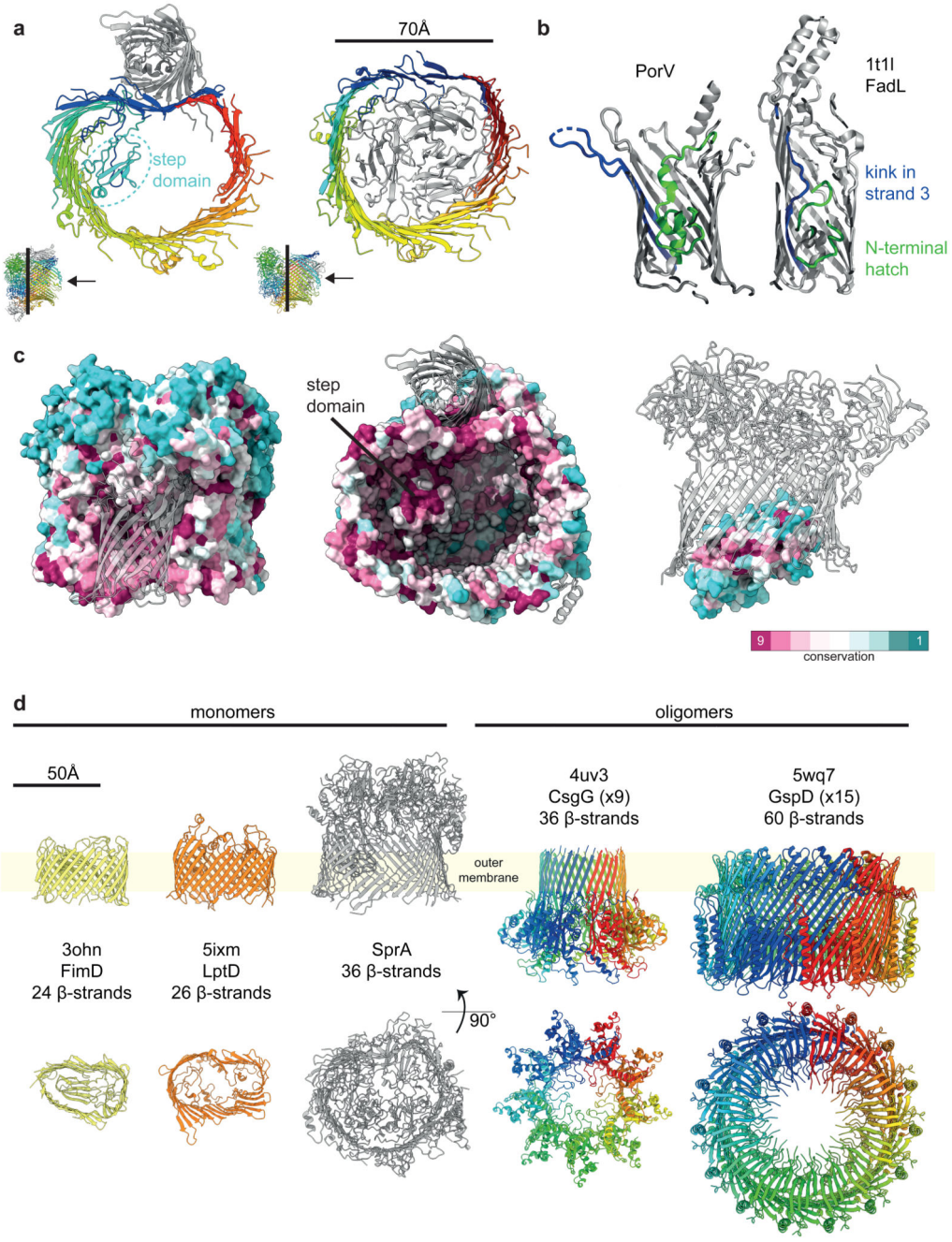

Fig. 3. Structural analysis of the SprA translocon complexes.

a, SprA barrel morphologies in the PorV (left) and Plug complexes (right) viewed from the periplasm and with cap domains cut away for clarity (as shown in insert). PorV and Plug, grey. **b,** Structural comparison of PorV with FadL. **c,** Surface conservation of SprA (left and centre, shown in the context of the PorV complex) and Plug (right, shown in the Plug complex) as determined by Consurf[31]. **d,** Structural comparison of SprA with other large β-barrel bacterial outer membrane proteins.

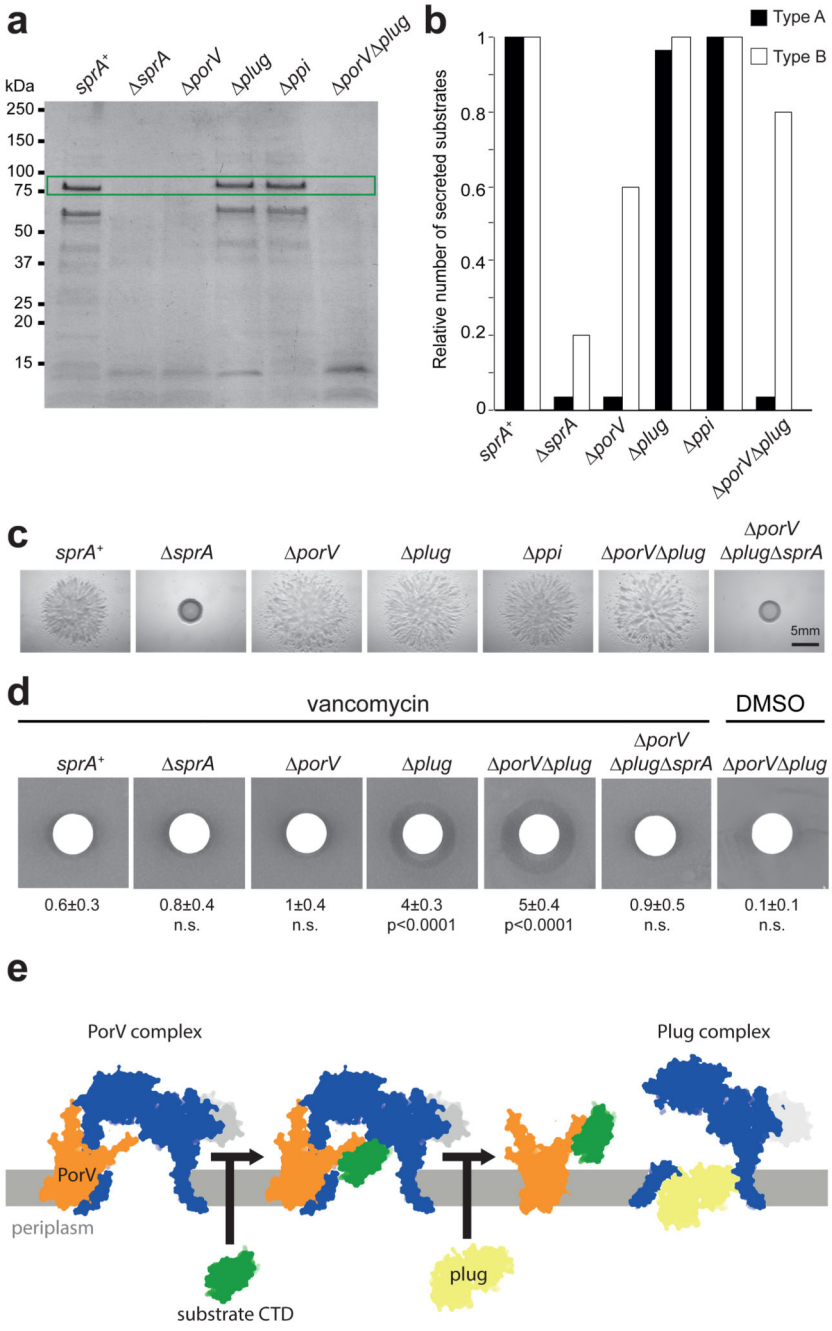

Fig. 4. Biological consequences of removing SprA partner proteins

a-b, Secretome analysis of culture supernatants. **a,** Coomassie-stained SDS-PAGE gel. The major T9SS-secreted chitinase ChiA is highlighted (green boxing). Similar data were obtained for three biological repeats. For gel source data see Supplementary Fig. 1. **b,** T9SS substrates detected by proteomics at >1% of the protein abundance in strain *sprA*$^{+}$, for which 30 Type A (TIGR04183 family) and 5 Type B (TIGR04131 family) CTD-dependent proteins were detected. **c,** Spreading (gliding) morphology of colonies on agar. Similar data were obtained for three biological repeats. **d,** Vancomycin sensitivity by disc diffusion assay.

Europe PMC Funders Author Manuscripts

Mean radius of inhibition **(mm)** ± S.D. measured from the disc edge (n=4 for Δ*porV* and Δ*plug*; n=5 otherwise), statistical significance by one-way ANOVA with post-hoc Dunnett's test using *sprA*$^{+}$ as control group, n.s. = not significant. **a-d,** *sprA*$^{+}$ strains express the Twin-Strep-SprA fusion. **e,** Model for the T9SS translocon mechanism.

Europe PMC Funders Author Manuscripts